Materials Characterization 215 (2024) 114234

Contents lists available at ScienceDirect

Materials Characterization

journal homepage: www.elsevier.com/locate/matchar

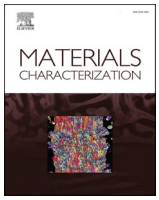

Nano-, micro- and macro-indentation tests of thermal spray WC-Ni coatings with lamellar microstructure at different particle deposition temperatures

J.R. Yuan, X.P. Zhu *, M.K. Lei *

Surface Engineering Laboratory, School of Materials Science and Engineering, Dalian University of Technology, Dalian 116024, China.

ARTICLE INFO

Keywords:
Indentation tests
Thermal spray
Cemented carbides coatings
Mechanical properties
Lamellar microstructure
Porosity

ABSTRACT

The mechanical properties of WC-Ni coatings by HVOF thermal spraying were comprehensively evaluated by indentation tests at a wide load range of 10^{-1}-10^{3} N, i.e. nano-, micro- and macro-indentations. The correlation between process parameters and coating microstructure and mechanical properties was characterized via particle deposition temperature. The coating microstructure changes in reduced porosity, enhanced WC phase decomposition and better splats flattening were correlated to the particle deposition temperature rising. A porosity divergence between coating surface and cross-section was found as a quantitative anisotropy indicator to coating intrinsic lamellar microstructure formed by the splats flattening and piling up. Considering the lamellar microstructure, indentation responses on coating surface and cross-section were compared for hardness and elastic modulus evaluation below 3 N. The surface hardness is higher than that of cross-section, and both increased correlatively to the particle deposition temperature rising except for the almost constant surface hardness below 1 N. An analogous particle temperature-dependent behavior was also manifested for the elastic modulus by nano-indentation below 1 N. Interestingly, the elastic modulus by coating surface micro-indentation at 30 N presented identical particle temperature dependence to that by coating cross-section nano-indentation, both consistently representing the overall coating elastic modulus change trend verified by non-destructive ultrasonic test. Indentation fracture toughness on coating surface under 1.96 kN and on coating cross-section under 49 N was comparatively evaluated, and the values had a reverse trend of dependence on the particle deposition temperature. The particle-deposition-temperature dependent mechanical properties were interpreted by the coating intra-splats and inter-splats defects reduction with enhanced carbide-metal bonding essentially determined by the melting state of the metal binder phase, providing an insight to utilize indentation tests for characterizing thermal spray coatings.

1. Introduction

The cemented tungsten carbides, also termed as hardmetals, are typically referred to as a hard material category of WC-Me system (Me: metallic binder phase of Co, Ni, Fe or their alloys etc.). A high content of WC hard phase over 70 wt% sintered with the metallic binders has been usually employed to provide a good combination of high hardness and moderate toughness intended for manufacturing tools or wear-resistant components in mechanical equipment [1,2]. In past two decades, intensive attentions have been paid on the research and development in industrial applications of these materials as protective coatings by thermal spray technology onto components for versatile wear-, corrosion-resistant and/or loading-bearing purposes etc. [3–5]. For efficient material utilization in the advanced manufacturing development in near future, the material-product-process linking should be addressed for realizing a knowledge-based manufacturing toward desired high performance of a product [6,7]. Up to now, the process development of the cemented carbides coatings mainly involves oxygen-acetylene flame spraying [8], plasma spraying [1,9], detonation spraying [10], and high-velocity oxy-fuel (HVOF) or air-fuel spraying (HVAF) [11,12] etc. A general principle of these thermal spray processes is that the WC-based particles by powder injection into the spraying flame are heated and accelerated, to a high-temperature and high-velocity, mostly in a semi-molten state, and then hit the surface of components to deform as flattening splats and solidify with fast cooling to form the coatings of layer-by-layer splats piling up. It is well known that, HIP sintering process, developed to manufacture bulk cemented carbides materials and parts, ensures their good mechanical properties with a highly

* Corresponding authors.
E-mail addresses: jryuan@mail.dlut.edu.cn (J.R. Yuan), xpzhu@dlut.edu.cn (X.P. Zhu), surfeng@dlut.edu.cn (M.K. Lei).

https://doi.org/10.1016/j.matchar.2024.114234
Received 24 April 2024; Received in revised form 12 July 2024; Accepted 31 July 2024
Available online 3 August 2024

densified and uniform microstructure by sufficient heating and pressing processes at equilibrium thermodynamic state. The thermal spray processes are considered as an efficient process for fast forming of cemented carbides as the coating form in an open air, by which a porous coating microstructure up to 10% porosity were commonly obtained dependent on the specific spray process employed for the manufacturing. Denser coatings with good bonding between the WC phase and the metal phase are expected to achieve high mechanical properties of deposited coatings for practical applications. Even for HVOF or HVAF, intentionally developed for depositing cemented tungsten carbide coatings with the highest particle velocity and moderate deposition temperatures, the well deposited coatings still have an averaged porosity at 1% order. Particularly, the thermal spray coatings have the featured lamellar structure from the layer-by-layer splats growth by the semi-molten particles impacting, where the microstructural defects of micropores/crevices, decomposition of stochiometric WC phase as a result of reaction between the high-temperature particles and ambient oxygen, mainly concentrated at the interface area between the splats, may significantly deteriorate the mechanical properties of coating hardness, elastic modulus, and fracture toughness etc., limiting the performances such as wear, corrosion and impact resistance of coated components [13–17].

Therefore, it is still difficult to effectively control and optimize thermal spray processes toward the high performance of components, due to the complicate interactions that a high particle temperature may enhance WC decomposition negatively affecting the mechanical properties, but better for splats deformation and coating densification beneficial to the properties [10]. In this regard, recent research advances show process signatures a feasible tool for effective process optimization, as deriving a process-independent correlation on physical mechanisms for various processes to final performance of manufactured component via surface integrity, facilitating a material-product-process linking for advanced manufacturing of a product [18–20]. As for the coated components, the coating mechanical properties with relevant coating microstructures could be the major surface integrity parameters determining the product wear and/or impact resistance performance, and the process signature analysis is to establish a quantitative correlation between the major surface integrity parameters to the coating deposition temperature and stress field or in a form of material internal energy. Once a process signature correlation to major surface integrity parameters that determine a desired performance is identified, thermal spray processes could be effectively optimized according to the required particle temperature and velocity that can be also online monitored to control the coating deposition. Consequently, more accurate and advanced evaluation approaches for coating mechanical properties are indispensable to post the process signature correlation for optimization of various thermal spray processes [21]. The indentation tests are recognized as a versatile and efficient method for analyzing the mechanical properties of coatings, practically convenient to be widely applied in industrial sectors [10,13,16,21–24]. The hardness measurements of cemented carbides were mainly performed using a squared-based, pyramidal-shaped diamond Vickers indenter, where micro-indentation test with a load of 0.3 kgf (2.94 N) was commonly adopted for thermal spray coatings [10,16,22]. Here, both units of kgf and N are described for a comparison purpose among different studies. Elastic modulus of coatings is mainly measured by using nano-indentation with trihedral diamond Berkovich indenter under loads typically in 100 mN order [16,24,25], or occasionally Vickers indenter may be applied [23]. The fracture toughness measurements of coatings were carried out using Vickers indenter, with a higher testing load in a range of 2–5 kgf [13,23].

Suresh Babu et al. [10] evaluated detonation-sprayed WC-12Co coatings of 350 μm in thickness by indentation tests to obtain representative hardness and modulus of the coatings. A representative Vickers hardness was derived to represent the mechanical property of a substantial volume of the coatings, by characterizing the hardness as a function of normalized indentation depth on coating surface and cross-section. Appropriate test loads were found for the hardness test as 5–10 kgf on the coating surface and of 2–5 kgf on the coating cross-section, respectively, to exclude so-called indentation size effect. However, the elastic modulus extracted from nano-indentation under 0.3 kgf and 0.9 kgf did not exhibit the indentation size effect as that of hardness measurement. Houdková et al. [26] conducted instrumented indentation tests by nano-indentation with Berkovich indenter on different HVOF-sprayed cemented carbides coatings in thickness of 300–500 μm. The hardness was measured continuously on the polished coating cross-sections as a function of indenter penetration depth at loads from 20 mN to 10 N. The authors concluded that the values of hardness and elastic modulus tested under a load corresponding to indentation depths no less than 2 μm were considered as the representative properties of the entire coatings. Barbera-Sosa et al. [27] reported indentation size effect with an indentation depth less than 1.5 μm for the nano-indentation tests, on both the surface and cross-section of HVOF-sprayed WC-12Co (300 μm) and WC-10Co-4Cr (500 μm) coatings; meanwhile, the hardness and elastic modulus tested on the coating surfaces higher than those on the coating cross-sections. Vickers microhardness tests at loads of 0.49–2.94 N were employed in our previous study to characterize WC-10Ni coatings on their polished surfaces, and the lower hardness measured under the higher loads was mainly ascribed to the large indentation contact area covering enough distribution of coating porosity and WC phase retention [28]. The thickness of thermal spray coatings for various applications ranged across 0.1–1 mm, and the coating microstructures of hard phase and metal binder phase, flattened particles, micropores have the typical size scale from submicron to hundred microns. The distribution of oriented microstructure with lamellar features spanning in the characteristic scale of 3–4 orders of magnitude, complicates the evaluation of coating mechanical properties by indentation tests and even causes controversial results under different indentation loads.

In this work, the indentation tests with either Vickers or Berkovich indenter, were comprehensively studied to evaluate the mechanical properties of hardness, elastic modulus, and fracture toughness, by employing a load across 4 orders of magnitude from 100 mN to kN referred to as nano-, micro- and macro-indentation tests, respectively. For this purpose, WC-12Ni coatings are prepared by regulating HVOF process parameters according to deposited temperature of WC-12Ni particles to obtain coatings of various microstructures at a constant spraying distance, while keeping almost the same particle deposition velocity. To derive the underlying correlation between the process parameters and the indentation-extracted mechanical properties via particle deposition temperature, the variations of mechanical properties were probed by the specific indentation responses on characteristic microstructures under different particle deposition temperatures, in combination with comparative analysis of non-destructive tests. The appropriate selection of indentation methods was discussed for quantitative evaluation of mechanical properties of thermal spray coatings considering their intrinsic lamellar features by the splats flattening and piling up.

2. Experimental procedures

2.1. Sample preparation

Coatings were prepared by the Metco LF EvoCoat thermal spray system equipped with a Woka-610-Si HVOF spray gun on 17-4PH precipitation-strengthening martensitic stainless steel samples using commercial WC-12Ni powders (WEL 46112–22) of −45 + 15 μm. In-flight particle velocity and temperature diagnostics were performed using OSEIR Spray Watch 2S for the spray distance of 350 mm. The particle deposition temperature is thus controlled by appropriately adjusting the oxygen and fuel ratio O/F(λ) value, while keeping the particle deposition average velocity basically the same at the fixed spray distance. The selected process parameters for coating preparation were shown in Table 1. The thickness of as-deposited coatings was around

Table 1
Process parameters of HVOF sprayed WC-12Ni coating adjusted by O/F(λ) to achieve desired particle deposition temperatures at the same spray distance of 350 mm.

No.	Oxygen flow (NLPM)	Kerosene flow (L/h)	Spray distance (mm)	O/F(λ)	T_{mean} (°C)	T_{SD}	V_{mean} (m/s)	V_{SD}
T1	811	22.7		1.05	1680	3.0	908	11.6
T2	888	22.7		1.15	1646	5.2	912	5.1
T3	890	21	350	1.25	1594	4.4	912	11.7
T4	960	21		1.35	1558	2.4	914	9.9
T5	950	19.3		1.45	1490	10.0	908	7.2

250 μm, and finally polished down to 200 μm for testing.

2.2. Microstructure characterization

The microstructure of the surface and cross-section (parallel to the scanning direction of the gun) of coatings were characterized using a Zeiss SUPRA55 field-emission scanning electron microscope (Carl Zeiss, Germany) and JXA-8530F Plus field-emission electron probe (JEOL, Japan) at an accelerating voltage of 15 kV. The porosity on surface and cross-section of coatings was measured using the image analysis software Image J (National Institutes of Health, USA), and the images at 400× magnification of eight sites were randomly selected for each sample observation. The X-ray diffraction measurement using XRD-6000 diffractometer (Shimadzu Production Institute, Japan) with Cu Kα radiation was carried out to analyze the phase structure of feedstock powder and coatings in scanning range 20–100°. Estimation of the relative contents of the WC and C-deficient phase was calculated from the integrated area of the strongest diffraction peaks to characterize the decomposition of WC-12Ni coatings, e.g. the retention of WC was calculated by [29].

$$I_{ret,WC} = \frac{I_{WC}}{I_{WC} + I_W + I_{W_2C} + I_{WC_{1-x}}} \quad (1)$$

where the I_{WC}、 I_W、 I_{W2C} 、$I_{WC1\text{-}x}$ correspond to integrated area of the strongest diffraction peaks of WC at $2\theta = 35.6°$, W_2C at $2\theta = 39.4°$, W at $2\theta = 41.6°$ and $WC_{1\text{-}x}$ at $2\theta = 42.9°$, respectively.

2.3. Indentation tests

The nano-indentation measurement was performed using the Nano-indenter XP 100BA-1C (MTS, USA). A trihedral diamond Berkovich indenter was applied to the polished coatings, with a fixed maximum load of 650 mN during the test. An array of 9 indentations in a 3×3 matrix with 60 μm spacing was made on the coating surface and a 2×4 matrix was made on the coating cross-section of each sample, with a maximum penetration depth of about 2000 nm. The nano-indentation hardness (GPa) and elastic modulus (GPa) values were calculated based on the penetration depth using the Oliver-Pharr method [26]. Micro-hardness test of the coatings was carried out on the polished surface and cross-section of the coatings using HXD-1000TM Vickers indentation tester (Shanghai Taiming Optical Instruments Co., Ltd., China) under a load of 0.49 N and 2.94 N with 10 s dwelling time, and hardness values were averaged at least 10 measurements. The hardness of the coating cross-section was measured at the center of the entire thickness, i.e. position at approximately 100 μm from the surface of the coating. Instrumented micro-indentation test was performed using a Berkovich indenter MFT-4000 Multi-functional Material Surface Property Tester (Lanzhou Huahui Instrument Technology Co., Ltd., China), on the polished coating surface at 30 N load. The elastic modulus was calculated following the Oliver-Pharr method, at least 6 indentations were conducted on each coating surface.

The fracture toughness (K_{IC}) on coating cross-sections and surfaces was tested under a load of 49 N and 1.96 kN, respectively using Vickers hardness testers of a 200HVS-10 type and a HV-250TVS type (Laizhou Huayin Experimental Instrument Co., Ltd., China). The high load of 1.96 kN was selected according to occurrence of surface radial cracks along the diagonal of the indent of indentation for all the tested coatings. For each coating, 5 measurements were made under each load and the space between two adjacent indentations was approximately 5 times the indent diagonal. The fracture toughness of the coating cross-sections and surfaces was assessed using two different crack opening modes proposed by Anstis [30] (median/radial cracks, when the cracks are also developed under the indent and completely surround the indentation) and Niihara [31] (Palmqvist cracks, when the cracks are only generated at the extremities of the indent). The Anstis's equation is described as

$$K_{IC} = 0.016\left(P/c^{3/2}\right)(E/H)^{1/2} \quad (2)$$

where the P is indentation load (N), H the Vickers hardness (GPa) at a load of 2.94 N, E elastic modulus (GPa), c average half-length of crack extending along the indent diagonal (μm). The Niihara's equation is

$$\left(K_{IC}\Phi/Ha^{1/2}\right)(H/E\Phi)^{2/5} = 0.035(l/a)^{-1/2} \quad (3)$$

where the Φ is constraint factor ($=H/\sigma_y \approx 3$, where σ_y is the yield stress), a indent half-diagonal (μm), l Palmqvist crack length (μm).

2.4. Non-destructive tests

The third method of coating elastic modulus test was the non-destructive ultrasonic testing. The transverse v_s and longitudinal v_l wave velocities passing through the coating were recorded by the ultrasonic water immersion focusing probe, and the elastic modulus E and Poisson's ratio σ can be calculated by Eq. (4), where ρ is the coating density [29].

$$E = \frac{\rho v_s^2\left(3v_l^2 - 4v_s^2\right)}{v_l^2 - v_s^2}, \sigma = \frac{\left(v_l^2 - 2v_s^2\right)}{2\left(v_l^2 - v_s^2\right)} \quad (4)$$

Residual stress on the surface of WC-12Ni coatings was measured using non-destructive x-ray residual stress testing on a Pulstec μ-360s equipment based on a cosα method. A fixed X-ray incident angle of 30° to sample surface was used. In the cosα method, X-rays are 360°-omni-directionally diffracted from the sample's polycrystalline structure around the path of incident X-rays and the complete Debye-Scherrer ring are detected by the two-dimensional detector [32]. The residual stress is evaluated using the data from the sample at 125 points around the Debye-Scherrer ring.

3. Results and discussion

3.1. Coating microstructure

Fig. 1 shows XRD patterns of the feedstock powders and the WC-12Ni coatings deposited at different particle deposition temperatures of 1490–1680 °C, respectively. For all the particle deposition temperatures, carbon-deficient phases of close-packed hexagonal structure W_2C, cubic $WC_{1\text{-}x}$, and body-centered cubic structure W were detected as a result of high-temperature oxidative decarburization of the original hexagonal structure WC phase. The relative contents of these phases derived from the XRD results, are presented in Fig. 2. As the particle deposition temperature increases, the WC phase retention keeps

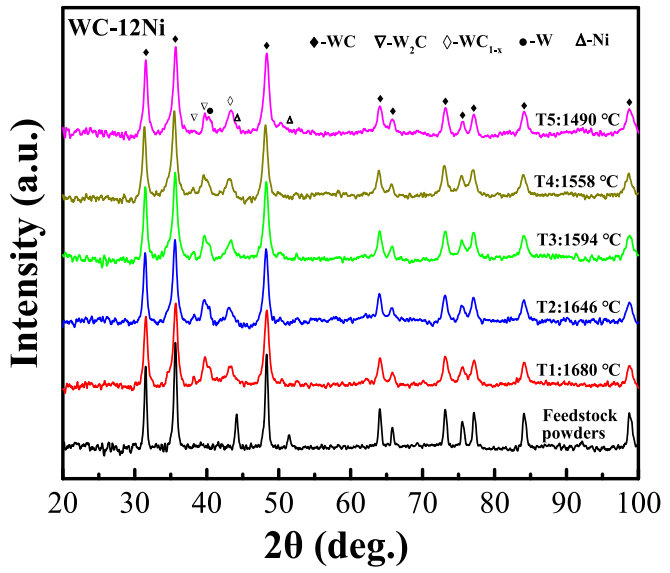

Fig. 1. XRD patterns of WC-12Ni coatings at the different particle deposition temperatures and feedstock powders.

approximately 86% for the deposition temperatures no more than 1600 °C, and rapidly drops to about 80% at the higher temperatures up to 1680 °C [Fig. 2(a)]. Along with the reduction of WC phase content at higher temperatures due to its increased decarburization, the contents of carbon-deficient phases W_2C and W correspondingly increase, however, that of WC_{1-x} phase generally shows a decreasing trend. It is indicated that, the stable phases of W_2C and W are preferably formed over the metastable WC_{1-x} from the decarburization reaction of WC phase at the higher particle temperatures.

Fig. 3 shows the backscattered electron images to reveal typical microstructural morphology on the polished cross-section of WC-12Ni coatings at the selected particle deposition temperatures of 1680, 1594 and 1490 °C respectively, representing the highest, medium, lowest ones of this study. In general, the images at lower magnification present the morphology of coating lamellar feature formed by the splats flattening and piling up with inter-splats boundaries indicated by dotted curves, and those at higher magnification give the detailed inter-splats and intra-splats features of WC grains with C-deficient phases and Ni binder phase. The particle deposition temperature had a strong influence on the coating morphological features. The WC grains after decarburization clearly show a core-shell structure where the brighter shell is imaged from the C-deficient phases of WC_{1-x}, W_2C, and W due to their higher backscattered electron emission than that of WC phase. Moreover, some small WC grains had fully converted to brighter in the morphology imaging, as a result of C loss by decarburization. These decarburization features are concentrated along the inter-splat boundaries, implying that the notable oxidation took place on the surface of each WC-Ni feedstock powders heated to the high temperatures by the thermal spray jet or plume during their flight and deposition. For the WC-12Ni coatings of the highest particle deposition temperature of 1680 °C, many big WC grains have core-shell structure, whereas for the other two coatings, only small core-shell WC grains were observed along with some WC grains of partial shell structure, confirming the less oxidization at the lower particle deposition temperatures. Furthermore, inter-splat pores and cracks were apparently presented in the coating of lowest particle deposition temperature of 1490 °C, attributable to insufficient melting of Ni binder phase. In addition, some broken WC grains can be found in all the coatings as a result of the high-velocity impacting effect by the particle deposition velocity of about 900 m/s.

Fig. 4 shows the dependence of coating porosity on the particle deposition temperature. The porosity of all the coatings measured from both the coating surface and cross-section was obtained by image analysis on the morphology of secondary electron images at 400× magnification. The coatings have a relatively low porosity well distributed below 2%, as a merit of the high particle velocity of HVOF process over the other thermal spray processes. It is clearly revealed that, by controlling the same particle velocity, i.e. about 900 m/s in this case, the particle deposition temperature rising led to a notable reduction of coating porosity. Note that, a porosity divergence between coating surface and cross-section is found on both the absolute value and the reduction tendency on the particle deposition temperatures. The overall porosity of coating surface is lower than that of coating cross-section, except for a similar value at the lowest temperature of 1490 °C. The porosity observed on the coating cross-section demonstrates a linear reduction of the averaged values from about 1.2% at 1490 °C to 0.9% at 1646 °C, followed with a rapid drop to 0.5% at 1680 °C, in contrast, the value on the coating surface shows a rapid drop from about 1.2% at 1490 °C to 0.4% at 1558 °C followed with a linear reduction to 0.2% at 1680 °C. With the microstructural morphology observation on coating cross-section (Fig. 3), it is shown that, the porosity divergence may be employed as a quantified anisotropy indicator of the lamellar structure features of thermal spray coatings. For instance, the anisotropy of coating lamellar microstructure is relatively low in the cases of the lowest temperature of 1490 °C and the highest temperature of 1680 °C, i.e. the difference between the surface and the cross-section porosity is lower, as compared to those of the intermediate temperatures.

The coating microstructures correlation to particle deposition temperature is understood in two aspects. On one hand, the higher particle deposition temperatures enhance the oxidative decarburization reaction with more release of gaseous by-products. The oxidative reaction mainly took place at the surface of high-temperature particles in contact with entrapped ambient air in the jet flow of particle deposition [29,33], leading to formation of coating micropores concentrated along the inter-splat regions during coating growth by the splat piling-up. On the other

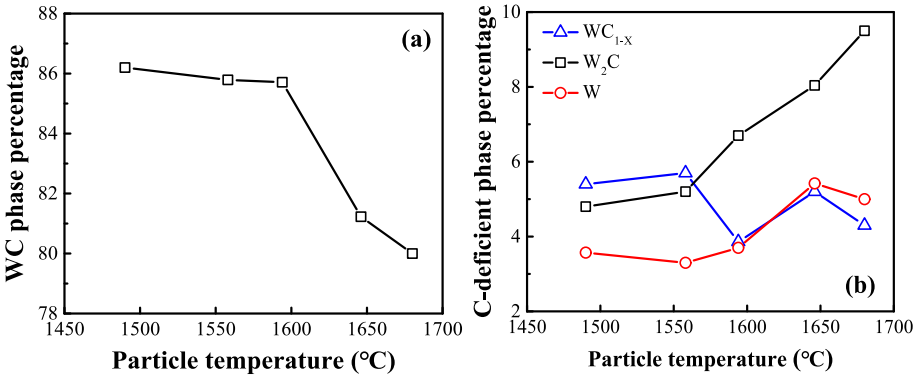

Fig. 2. Dependence of phase percentage in WC-12Ni coatings on the particle deposition temperature: (a) WC phase, (b) W_2C, W, WC_{1-X} phases, respectively.

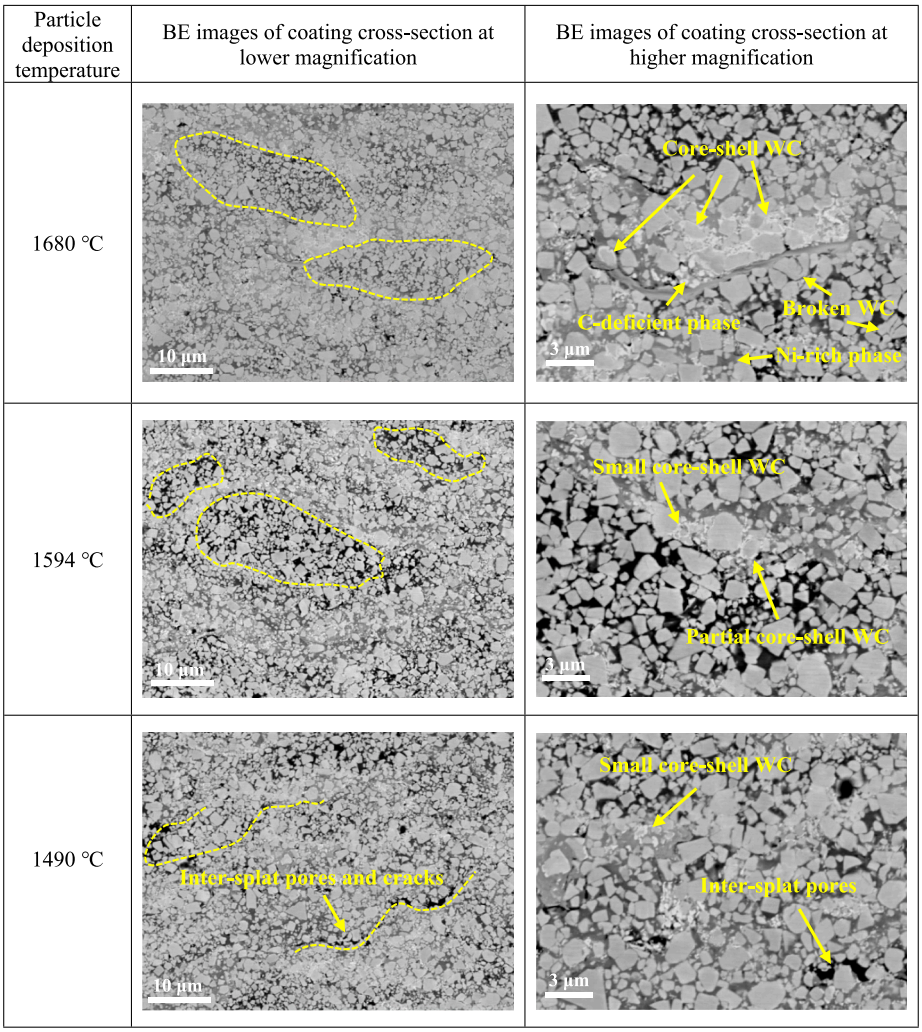

Fig. 3. The cross-sectional morphologies by backscattering electron images of WC-12Ni coatings, where the arrows indicate the WC grains of different features, Ni enrichment, inter-splat pores and cracks, and the dotted curves indicate approximately inter-splat boundaries.

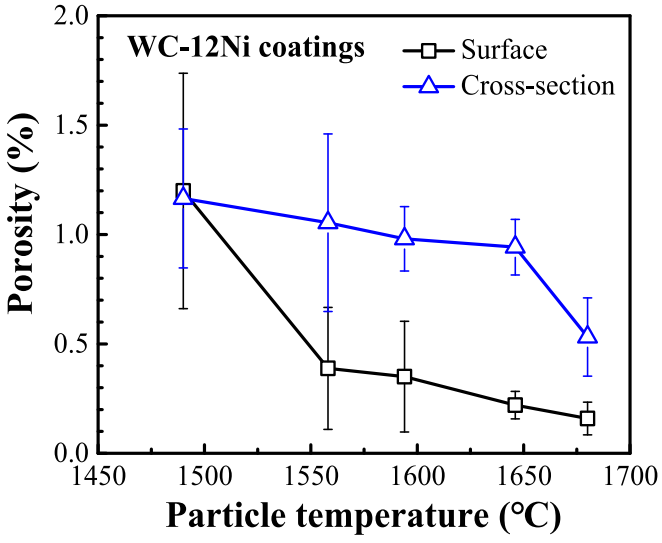

Fig. 4. Dependence of coating porosity of surface and cross-section for WC-12Ni coatings on the particle deposition temperature.

hand, the higher particle deposition temperatures promote melting of WC-Ni particles, especially, ensuring the Ni binder phase into a sufficiently molten state beneficent to better splat flattening upon high-velocity particle impacting deposition resulting in a more compact splat piling-up, as well as to the local WC/Ni phase interface bonding by molten Ni wetting on WC grains. Consequently, the anisotropy of coating porosity, i.e. the coating surface porosity lower than its cross-section value, may be understood as follow. The surface porosity is counted from the top surface view of pancake-like spreading morphology of flatten splats in diameter up to 100 μm order [34,35] by which the intra-splat area (splat interior) is dominant over that of inter-splat boundary, whereas the cross-section porosity is from side view of the piling-up flatten splats as a thin layer of several-μm thickness by which the counted areas for intra-splat interior and inter-splat boundary is comparable. The coating porosity anisotropy on the surface and cross-section is determined by the difference in defects density of pores and/or cracks within the intra-splat and inter-splat regions of flatten splats.

Both the intra-splat and inter-splat regions of coatings have continuous reduction of defects due to increased particle deposition temperature (Fig. 4). Specifically, an out-of-sync temperature-dependent rapid drop of coating porosity was revealed for the WC-12Ni coatings surface and the cross-section, presenting the lower coating anisotropy or better isotropy at the lowest and the highest particle deposition temperature to that of coatings at the intermediate temperatures. It is implied that the intra-splat and inter-splat regions within the coating surface and cross-

section had a comparable defect density at the lowest or highest particle deposition temperatures. The particle temperature effect on coating microstructure variations could be quantitatively explained considering the Ni binder phase melting point of 1455 °C. The turn-point of surface porosity rapid drop starting at the particle deposition temperature of 1558 °C is attributed to onset of well-molten Ni binder as heated up to about 100 °C higher of the binder melting point for sufficient wetting of WC and Ni phases within the particles that accounts for rapid reduction in intra-splat defects. Subsequently, the abrupt drop in coating cross-section porosity at 1646 °C is attributed to inter-splat defects minimized effectively by the further enhanced molten state of the binder phase, i.e. about 200 °C over its melting point that enables the binder wetting of depositing particles to previously solidified splats during piling-up. In a summary, the effect of particle deposition temperature on the microstructure of thermal spray cemented carbide coatings with laminar features is manifest from the occurrence of a two-stage coating defect reduction process i.e. intra-splat defect reduction onset at about 100 °C higher than the melting point of Ni, followed by inter-splat defect reduction at about 200 °C over its melting point, with the WC hard phase kept in solid state. It is essentially depending on melting state of the metal binder phase.

Surface integrity parameters of a coated component that determine the desired component final performance in service could be categorized as the surface features and surface characteristics of the component, where the former includes parameters describing surface finish and composition, and microstructure etc., and the latter includes those of surface physical and chemical properties [36]. Conventional study on effect of thermal spray processes on the coated component performance was recognized as a black-box relation or empirical relation employed for process optimization by trial-and-error method. In contrast, the process signatures correlation analysis can bridge the determining surface integrity parameters of desired performance to the process parameters of available manufacturing methods through external processing load and/or internal material loading on thermodynamic mechanism [18–20]. The WC-12Ni particle deposition temperature is posted as a characteristic material loading to derive process signature correlation for thermal spray process parameters. At first, the features of coating microstructures with porosity and phase composition were evaluated to post their correlation to the particle deposition temperature. The variations of WC retention ratio with carbon deficient phases and porosity of WC-12Ni coatings are strongly dependent on particle deposition temperature (Figs. 2 & 4). Particularly, the intrinsic lamellar microstructure with flattened splats for thermal spray coatings can be quantified by the anisotropy of the porosity divergence between coating surface and cross-section in correlation to the particle deposition temperature.

3.2. Coating mechanical properties

3.2.1. Hardness

Fig. 5 shows the hardness of WC-12Ni coatings tested under small loads of less than 1 N, in correlation to the particle deposition temperature, using the nano-indentation (Berkovich diamond indenter, 650 mN) and micro-indentation (Vickers diamond indenter, 0.49 N), respectively. The hardness on coating surface and cross-section were tested and compared for both the test methods, presenting a similar temperature-dependent behavior except for the higher absolute values of the Berkovich indenter data. The hardness on coating cross-sections increased correspondingly with the particle deposition temperature rising, i.e. nano-hardness increased from 10.8 GPa to about 13.4 GPa, and the micro-hardness ($HV_{0.49N}$) increased from 9.6 GPa to 10.7 GPa; whereas both the surface hardness kept almost unchanged with the particle deposition temperature change, around 13.3 GPa of the nano-hardness and 11.1 GPa of the micro-hardness ($HV_{0.49N}$), respectively. Note that, for the micro-hardness ($HV_{2.94N}$) at the higher indentation load, both coating surface and cross-section presented a consistent hardness increase to the particle deposition temperature rising, as shown in Fig. 6. The surface hardness increased from 9.2 GPa to 10.3 GPa, while the cross-section hardness from 8.6 GPa to 10.3 GPa.

Fig. 7 shows the secondary electron images of nano-indentation

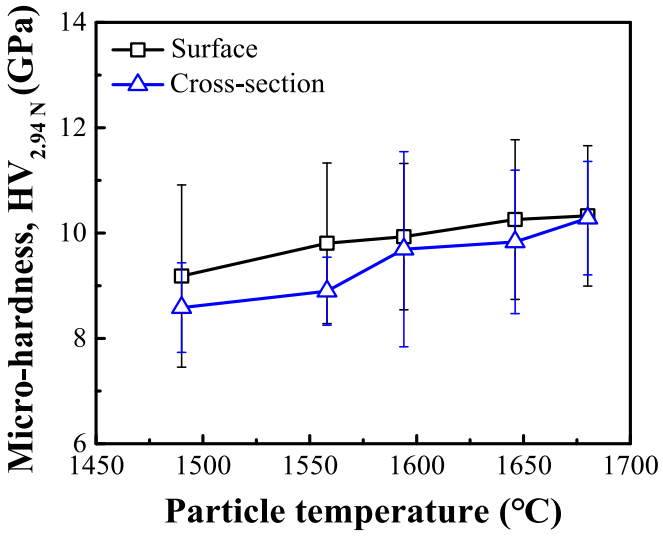

Fig. 6. Variation of the micro-hardness of WC-12Ni coatings under 2.94 N load at the different particle deposition temperatures.

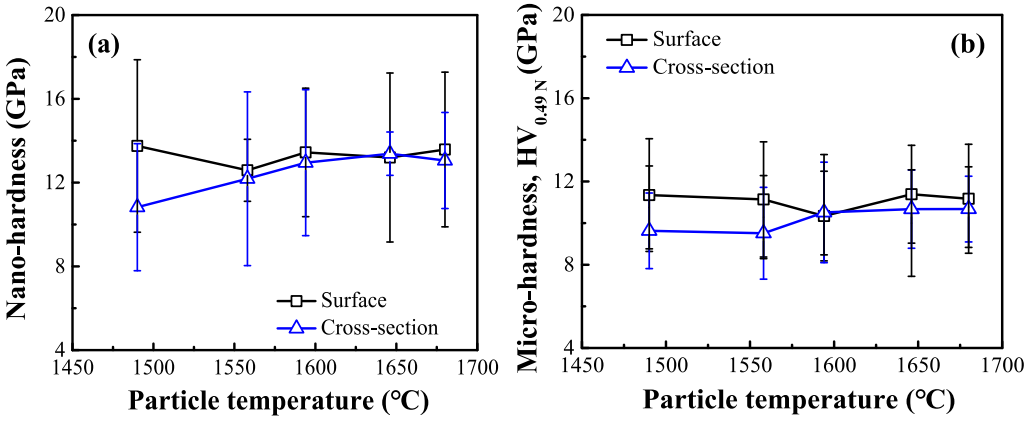

Fig. 5. Variation of the hardness of WC-12Ni coatings under two different small loads at the different particle deposition temperatures: (a) nano-hardness 650 mN, (b) micro-hardness 0.49 N.

indents, of the Berkovich indenter, on the surface and cross-section of coatings at the highest, medium, lowest particle deposition temperatures of 1680, 1594 and 1490 °C, respectively. The indents on the coatings at the particle deposition temperature of 1680 °C show a morphology of trihedral shape with clear and intact edge. It should be noted that, the micro-damage features of WC grains "buckling" and cracking at the edges of indents were found on the coatings at both 1594 and 1490 °C cases. The buckling of hard WC grains was caused by the action of bending moment during the indenter impressing, indicating the weaker bonding between WC and Ni binder formed under the lower particle deposition temperatures. Furthermore, a more weaker bonding feature between WC and Ni binder was identified as spalling of WC grains at the indent edges for the coating of the lowest particle deposition temperature of 1490 °C.

It is clearly shown that, the dependence of coating cross-section hardness increment on the particle deposition temperature rising has a convergence to the surface hardness, i.e. the hardness difference between the coating surface and the cross-section is reduced at the higher particle deposition temperatures. This phenomenon seems to be not consistent with the changing tendency of coating lamellar microstructure anisotropy that the porosity difference on coating cross-section and surface is larger at the intermediate temperatures (Fig. 4). It is implied that the hardness tested under the small loads is not solely affected by the temperature-dependent porosity, and the other factors should be considered.

3.2.2. Elastic modulus

Fig. 8 shows the results of elastic modulus of WC-12Ni coatings at the different particle deposition temperatures, obtained by nano-indentation and micro-indentation in comparison with that by ultrasonic test. The influence of particle deposition temperature on the nano-

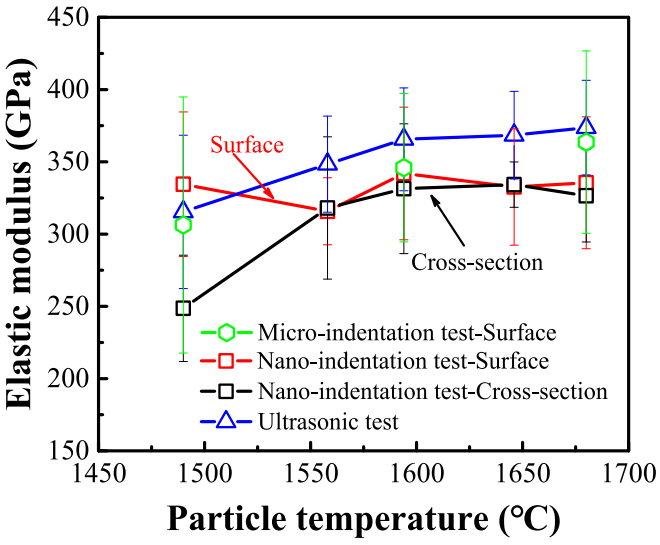

Fig. 8. Dependence of indentation-extracted elastic modulus on the particle deposition temperature for WC-12Ni coatings, in comparison with that of ultrasonic test method.

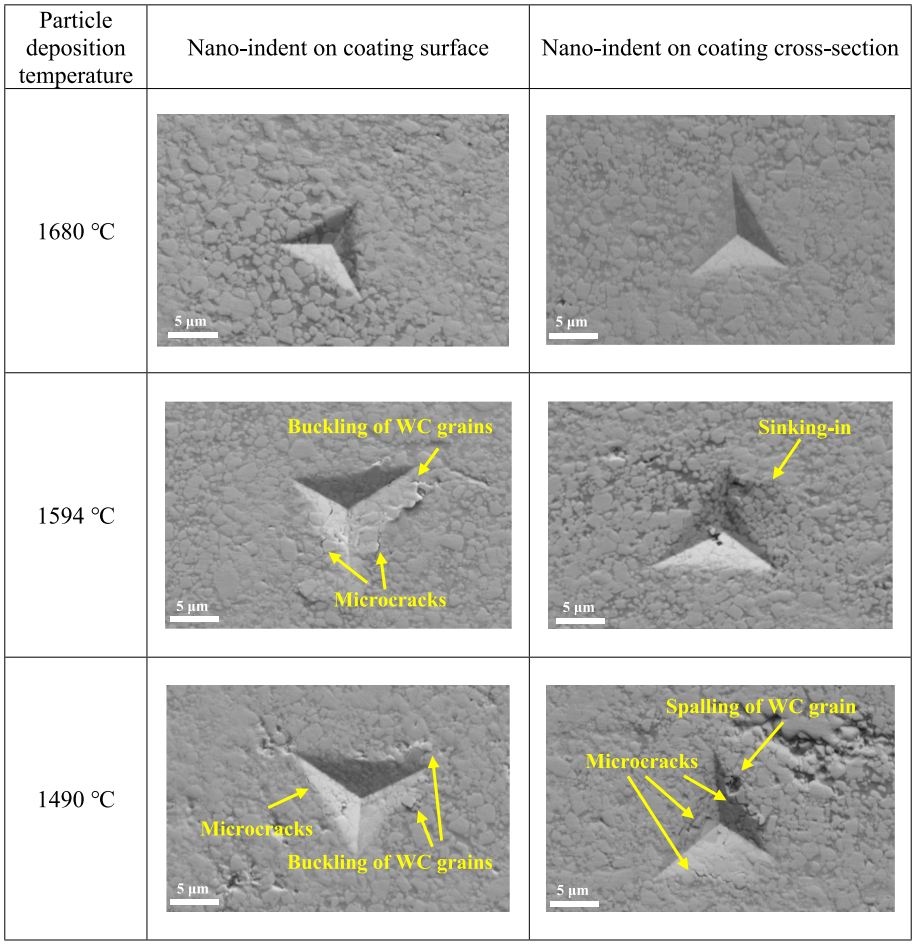

Fig. 7. The typical morphologies by secondary electron images of nano-indentation indents on surface and cross-section of WC-12Ni coatings at the selected particle deposition temperatures that represent the highest, medium, lowest ones of this study.

indentation elastic modulus presented the same changing trend as that of nano-hardness, i.e. the values measured on coating surface were insensitive to the temperature, whereas that on coating cross-section increased correlatively with the temperature rising. Specifically, the elastic modulus tested on coating surface by nano-indentation, denoted as $E_{s,nano}$, has a little variation within the range of about 315–341 GPa, whereas the values on coating cross-section as $E_{c,nano}$ increase from 249 GPa at 1490 °C to about 330 GPa at 1594 °C and above, converging to the range of $E_{s,nano}$. It is confirmed that, both the nano-indentation extracted hardness and elastic modulus on the coating surface and cross-section have the same temperature-dependent changing trend, presenting an anisotropy of coating mechanical properties.

The elastic modulus on WC-12Ni coating surfaces by using instrumented micro-indentation was measured at load of 30 N, denoted as $E_{s,micro}$, by which the representing coatings were selected for the lowest, medium, highest particle deposition temperatures at 1490, 1594 and 1680 °C. The micro-indentation test of coating cross-sections is not applicable here since the noticeable cracks could be created on the coatings by this load nearly two-order magnitude higher than that of nano-indentation. Of importance, the micro-indentation $E_{s,micro}$ measured on coating surface has the same temperature-dependent increasing trend to that of the nano-indentation $E_{c,nano}$ on the coating cross-section, as the particle deposition temperature rises from 1490 °C to 1680 °C. Correspondingly, the $E_{s,micro}$ increased from about 306 GPa to 364 GPa, with the values slightly higher than $E_{c,nano}$ at the respective particle temperatures. To better understand the good agreement between $E_{s,micro}$ and $E_{c,nano}$ as both differing from the $E_{s,nano}$ on coating surface, the elastic modulus of the WC-12Ni coatings was also measured by ultrasonic technique for comparison [29], denoted as E_{UT}. A focused beam of ultrasonic waves with diameter of about 1 mm, about five times of the coating thickness, was employed to measure the coating elastic modulus with the wave propagating and reflecting between the coating surface and substrate, and thus the E_{UT} represents the overall or macro mechanical property of the coatings. It is interestingly to find out that, the E_{UT} verifies the particle-temperature-dependent behavior of $E_{s,micro}$ and $E_{c,nano}$, i.e. presenting a correlative enhancement from 315 to 374 GPa on the temperature rising, with the values slightly higher than those of $E_{s,micro}$.

Note that, there seems to be a reverse indentation depth effect occurred for the elastic modulus result (Fig. 8) in comparison to that of hardness (Figs. 5&6), i.e. the higher indentation load at 30 N gives a higher elastic modulus $E_{s,micro}$ over that of coating cross-section nano-indentation $E_{c,nano}$ at 650 mN though both the results in good correlation to the particle deposition temperature rising. The indentation depth at 30 N is about 6–9 μm, with an indentation response involving at least a layer of flatten splats, and thus give a value closer to the result of E_{UT} by ultrasonic test that responds to all layers of flatten splats through the entire coating, i.e. about tens layers for a coating of 200 μm thickness. The coating surface nano-indentation cannot derive the temperature-dependent behavior of coating elastic modulus due to the low penetration depth of 1.1–1.5 μm, leading to the insensitive change of $E_{s,nano}$ with respect to particle deposition temperature (Fig. 8). As mentioned above, the coating cross-section view exposes inter-splats interfaces that take a major portion on the whole cross-section area, and thus the coating cross-section nano-indentation can reasonably respond to the inter-splats interface bonding in correlation to the particle deposition temperature except for underestimation of the absolute values of elastic modulus. It is indicated that, appropriative selection of nano- and micro-indentation methods can correctly evaluate the effect of particle deposition temperature on the overall elastic modulus of thermal spray coatings for coated components. The consistency of the measurement results among the $E_{c,nano}$, $E_{s,micro}$ and E_{UT} verifies the promotion of the elastic modulus due to the increase in the inter-splat bonding strength of the splat piling up by increasing the particle deposition temperature.

The indentation tests have been employed for evaluating mechanical properties including hardness or elastic modulus of various coatings and thin films. However, the indentation methods with different loads complicated the results as well as their explanation where the so-called indentation size effect was typically involved [10,26,27]. An indentation size effect was reported for Vickers hardness of WC-12Co coatings deposited by detonation spraying that the indentation depth/coating thickness ratio on coating surface should be in the range of 0.04–0.1 to obtain representative hardness of entire coatings, specifically, under a load within the range of 5–10 kgf on coating surfaces; while no such size effect was observed for the elastic modulus measured using nano-indentation test under 0.3 and 0.9 kgf loads [10]. Nevertheless, indentation size effect for both hardness and elastic modulus evaluation was found with a transition depth of about 2 μm by instrumented nano-indentation test on the cross-section of different HVOF cemented carbides coatings including WC-12Co, WC-17Co, WC-20CrC-7Ni, Cr_3C_2-25NiCr, and (Ti,Mo)(C,N)-37NiCo, i.e. the representative indentation depth should be no less than 2 μm [26]. By using the same nano-indentation method for both hardness and elastic modulus, a smaller transition depth of about 1 μm was observed on coating cross-section for HVOF WC-12Co and WC-10Co-4Cr coatings, whereas a higher transition depth of about 1.5 μm was identified on coating surface [27].

To clarify the indentation size effect, the specific indentation loads, indenter types, and indent depths together with ratio to coating thickness are summarized in Table 2. For the surface and cross-section hardness of WC-12Ni coatings were comparatively tested under the nano-indentation and micro-indentation (Figs. 5&6), the indent depth was of 1.1–1.5 μm for the nano-indentation at 650 mN, and of 1.3–2 μm and 3.5–4 μm for the micro-indentation at 0.49 N and 2.94 N, respectively. In general, the indentation depth effect is confirmed by the hardness results for both Vickers and Berkovich indenters, i.e. a transition depth of 1.5–2 μm in reasonable agreement with the published data for cemented carbide coatings of the other researchers [26,27]. Furthermore, comparison of the above hardness values at different loads verifies the indentation size effect for the hardness results by Vickers indenter, i.e. the smaller indentation load, the higher the hardness. This is consistent with our previous results of HVOF WC-10Ni coatings [28,29], where a higher indentation load of 2.94 N on the coating surface led to the indents with diagonals of 20–25 μm, representing the coating Vickers hardness as both the influence of porosity and phase change could be primarily included, otherwise the hard carbide phases mainly take effect under the smaller load of 0.49 N with the diagonals of indents only about 6–8 μm. At the same time, the indentation size effect is also verified by the consistent results that nano-indentation with Berkovich indenter has a smaller indentation depth even under a slightly larger load of 650 mN than that of the 0.49 N load of micro-indentation with Vickers indenter as a result of the different indenter geometry, resulting in a higher hardness value for the former (Fig. 5). In this regard, the indentation size effect may be termed more reasonably as indentation depth effect.

Note that, a phenomenon of particle-deposition-temperature

Table 2
A summary of indentation test conditions and results for WC-12Ni coatings.

Mechanical properties	Load	Indenter type	Coating position	Indent depth (μm)	Ratio of indent depth to coating thickness
Hardness and/or elastic modulus	650 mN	Berkovich	Surface & cross-section	1.1–1.5	0.0055–0.0075
	0.49 N	Vickers		1.3–2	0.0065–0.01
	2.94 N	Vickers		3.5–4	0.0175–0.02
Fracture toughness	30 N	Berkovich	Surface	6–9	0.03–0.0045
	49 N	Vickers	Cross-section	14–15	0.07–0.075
	1960 N		Surface	131–133	0.655–0.67

dependent hardness and elastic modulus is revealed by the present study. The mechanical properties clearly associated with the coating lamellar microstructure in correlation to particle deposition temperature are posted by comparative analysis of the surface and cross-section indentation responses. With the indentation depth effect at the small loads of 650 mN and 0.49 N, both the nano-hardness and micro-hardness tested on the coating surface are insensitive to particle deposition temperature change, indicating the major contribution of hard carbide phases of WC, WC_{1-x}, W_2C etc. to the hardness at the shallow indentation depth; instead, the respective hardness values on the coating cross-section present a correlative increasing trend to particle deposition temperature rising (Fig. 5). It is inferred that, as for the microstructure changes discussed above, the area of inter-splats boundaries took a majority at the coating cross-section view, and significantly contributed to the hardness and elastic modulus results. As a result, a small indentation load less than 1 N or an indentation depth of about 1 μm is able to probe the effect of particle deposition temperature on the coating mechanical properties. It is also verified by the Vickers micro-hardness tested at a higher load of 2.94 N, both the values on coating surface and cross-section consistently increased in correlation to the temperature rising (Fig. 6).

Therefore, how to correctly evaluate the coating representative or overall mechanical properties determined by the typical microstructure of thermal spray coatings with laminar features using indentation methods, such as hardness and elastic modulus studied in this case? Combined with these results, it is confirmed that the extraction of coating representative mechanical properties by indentation methods relies on how much the coating microstructure features could be involved in the indentation responses. The contribution from majority of coating porosity at the inter-splats could be well included if the indentation depth from the coating surface approach to the layer thickness of the flattened splats, as the penetration depth for 2.94 N is about 3.5–4 μm (Table 2) comparable to the flattened splats thickness usually within a few micrometers, e.g. for WC-10Co-4Cr coatings, about 3–10 μm [34,35].

Following the discussion of representative mechanical properties evaluation, the term of overall coating mechanical properties is employed to distinguish localized mechanical properties. As revealed in this study, the involved indentation depth effect can be utilized to probe the localized coating mechanical properties associated with the lamellar microstructures. It is shown that the nano-indentation has an indentation depth less than the thickness of flattened splats, and thus the extracted mechanical properties tested on the coating surface is mainly due to the response of the WC-Ni intra-splat features dominating the surface area, while those on the coating cross-section to that of both the inter-splat and intra-splat WC-Ni features. This mechanism is applicable to both the mechanical properties of hardness and elastic modulus, where the values tested on coating surface with small loads are insensitive to the particle deposition temperature, but the results on coating cross-section positively depends on particle deposition temperature rising as the inter-splat bonding was enhanced at higher particle deposition temperatures (Figs. 5&8).

3.2.3. *Indentation fracture toughness*

In our previous studies, it was recognized that, indentation fracture toughness of WC-based thermal spray coatings plays a determining role of their final performance of wear resistance [29]. Here, indentation fracture toughness of coatings is also evaluated by adopting 49 N load on coating cross-section, and in addition, a much higher load of 1.96 kN is employed to the coating surface indentation considering the coated component impact resistance performance under surface impacting of loads kN order [37].

Fig. 9 shows the results of Vickers indentation fracture toughness K_{IC} calculated using the two different equations (Eqs. 2 & 3). Both the equations give the same dependence of K_{IC} on particle deposition temperature for both coating surface and cross-section just different in the absolute values. At the same high particle deposition velocity of about 900 m/s, the increase of particle deposition temperature led to a reduction of K_{IC} values on the coating surface tested under 1.96 kN. With the temperature increasing from 1490 °C to 1680 °C , the K_{IC} values of the coating surface decreased from 12.2 MPa·$m^{1/2}$ to about 5.8 MPa·$m^{1/2}$ by the Ansits's formula, and from 27.3 MPa·$m^{1/2}$ to about 15.8 MPa·$m^{1/2}$ by the Niihara's formula. In contrast, the K_{IC} values tested on coating cross-section under 49 N increased with particle deposition temperature rising, i.e. the values of Ansits's formula from 3.1 MPa·$m^{1/2}$ to 4.8 MPa·$m^{1/2}$, and of Niihara's formula from 3.9 MPa·$m^{1/2}$ to 5.6 MPa·$m^{1/2}$. Note that, the Vickers indentation for the coating fracture toughness measurements demonstrates a reverse response that surface indentation fracture toughness has a decreasing trend to the particle deposition temperature rising whereas the cross-section ones an increasing trend.

Both the cracking morphology of indents on the coating cross-sections and surfaces were observed and compared, to understand the responses of coating fracture toughness tests. Fig. 10 presents the typical morphologies of indents on coating cross-section under 49 N load, for the coatings of the highest and the lowest particle deposition temperatures, respectively. The coating cross-section indentation indents have a typical cracking feature with cracks preferably formed at the two lateral corners and extended parallel to the coating surface. The crack propagation paths of indentation on the WC-12Ni coatings cross-section are mainly of intergranular type of WC/WC and WC/Ni, especially for those deposited at lower particle deposition temperatures. As the bonding strength of inter-splats and intra-splats of coatings increased significantly at the highest particle deposition temperature, some transgranular cracks in WC and Ni phases also occurred, in which the brittle C-deficient phases formed on WC phase due to decarburization is also a

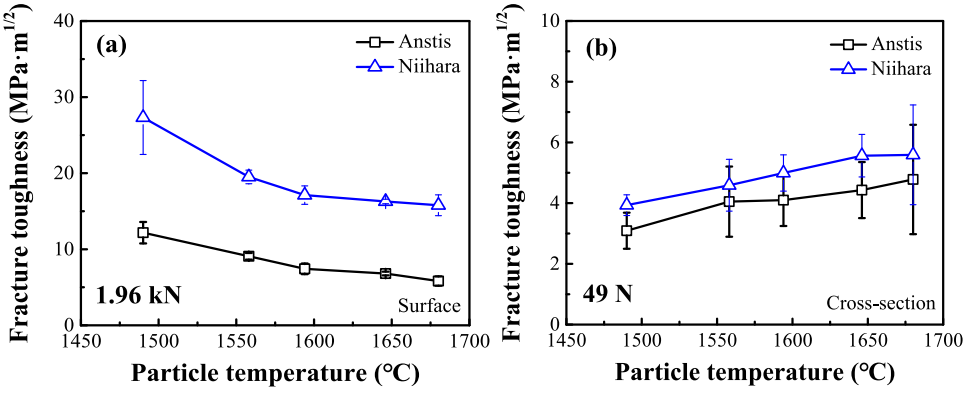

Fig. 9. Dependence of indentation fracture toughness on the particle deposition temperature for WC-12Ni coatings using various established formulations: (a) surface, (b) cross-section.

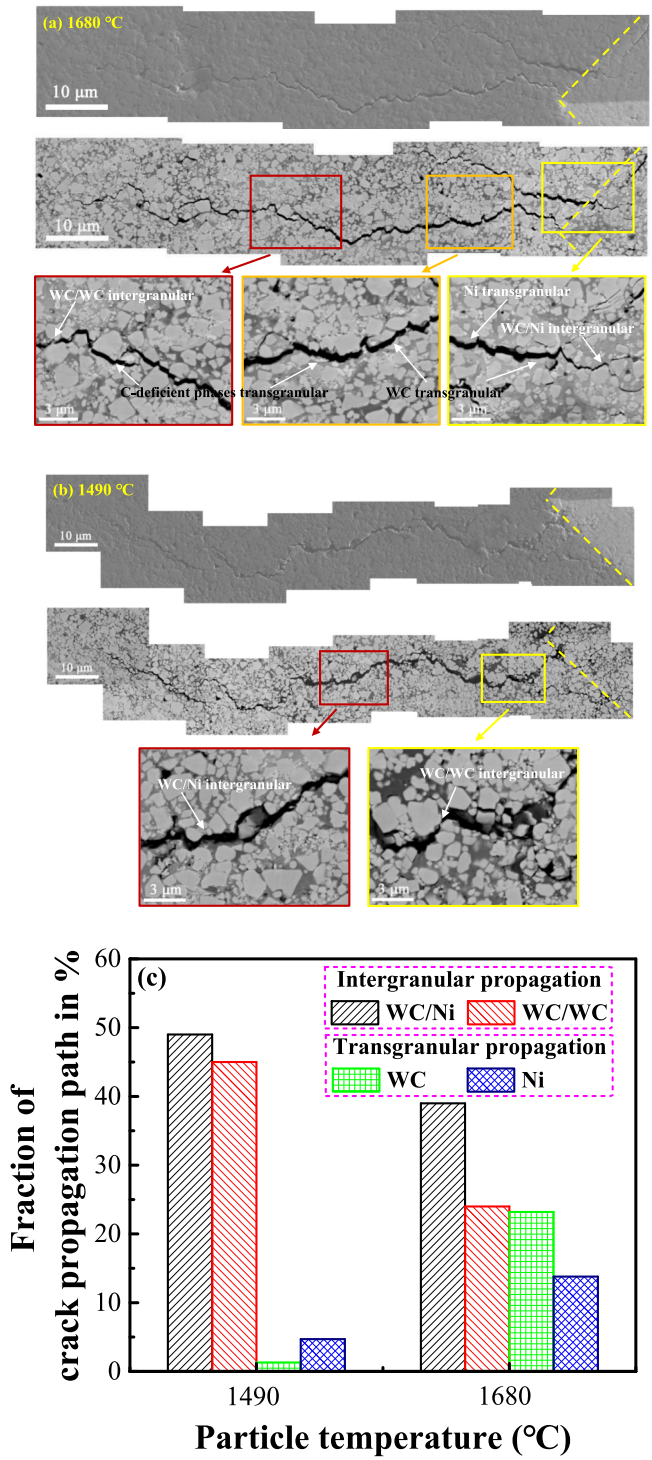

Fig. 10. The typical morphologies by both secondary electron and backscattering electron images of Vickers indents under 49 N for fracture toughness measurement on the cross-section of WC-12Ni coatings at the highest and lowest particle deposition temperatures, where the arrows indicate crack propagation paths of different types, and the dotted lines indicate indent edges: (a) 1680 °C, (b) 1490 °C, and (c) fraction of propagation length of different type cracks.

preferable transgranular cracking path. Moreover, the fractions of the four types crack propagation paths are determined according to the morphology images by measuring the cumulative crack lengths of each types to the total length of all types [Fig. 10(c)]. It is clearly seen that, for the coatings at lower particle deposition temperature of 1490 °C, the cracks propagated through the intergranular paths of WC/Ni and WC/WC interfaces took up about 94% of the total propagation length with the most preferable path of WC/Ni interface up to nearly 50% and the least transgranular WC cracking path was only of 1.7%. For the coatings at higher particle deposition temperature of 1680 °C, though the WC/Ni interface is most preferable cracking path, both the intergranular paths of WC/Ni and WC/WC were notably reduced to about 39% and 24%, and the transgranular cracking path through WC and Ni phases significantly increased to about 23% and 14%. The results confirmed that, the higher interfacial bonding strength between WC/Ni and WC/WC for the WC-12Ni coatings formed at the higher particle deposition temperature effectively restricted their intergranular cracking, and simultaneously enhanced probability of the transgranular cracking that was almost impossible for the lower particle temperature deposited WC-12Ni coatings with preferential cracking through the much weaker WC/Ni and WC/WC interfaces.

The morphologies of the Vickers indents on coating surface under 1.96 kN are shown in Fig. 11, at the highest, medium, and lowest particle deposition temperatures of 1680, 1594 and 1490 °C, respectively. Different from the lateral cracking morphology of coating cross-section indents, the surface indentation cracking on the coatings shows a typical feature of central symmetry to the four corners, i.e. all the corners have extended cracks with comparable lengths. In comparison, for more porous (less denser) coatings at lower particle deposition temperatures, more small segmented cracks was additionally generated within and/or around the indents.

Therefore, the indentation responses of coating fracture toughness tests could be interpreted in correlation to the coating laminar microstructure. At first, it is well recognized that the denser coatings have higher indentation fracture toughness tested on the coating cross-sections under 49 N due to the better inter-splats bonding with lower porosity at the higher particle deposition temperatures [Fig. 9(b)], in good agreement with previously work [28]. The reverse trend of indentation fracture toughness values by the indentation test on the coating surface is a new phenomenon as revealed in this study [Fig. 9 (a)]. As for evaluation of coating fracture toughness by indentation, interaction between the compressive stresses generated under the tip of the indenter perpendicular to the indentation surface and the pre-existing residual tensile stresses caused shear stresses within the coating, promoting the cracking underneath the indenter [38,39]. To check this effect, residual stresses on the coating surface were measured, as shown in Fig. 12. Small tensile residual stress was confirmed on all the coatings, showing a slight increasing trend from about 20 to 50 MPa with the increase of particle deposition temperature. As a result, the pre-existing stress mechanism is excluded for the temperature-dependent behaviors. Instead, the difference in the mechanical energy consumption of indentation process for the crack initiation/propagation could explain on abnormal behavior of the surface indentation fracture toughness. On one hand, the type of symmetrical cracking from all the four corners of indents should have shorter crack lengths as compared to that of only two lateral cracking under comparable condition because the consumed mechanical energy of cracking was divided to the four corner cracks initiation/propagation during the indentation process, as proved by the fact that surface fracture toughness values are always higher than those cross-section ones if adopting the same fracture toughness equations (Fig. 9); on the other hand, the less denser coatings at lower particle deposition temperatures have higher density of pore defects, on which densification of the coatings can consume a part of the indentation mechanical energy and simultaneously initiation/propagation of multiple cracks are preferably developed from the defect sites into the numerous segmented cracks during the indentation process, further limiting the corner crack propagation and resulting in much shorter corner cracks (Fig. 11). As a result, the fracture toughness of coating surfaces calculated by both the equations counting only the corner crack length presented a corresponding decreasing trend with the particle deposition rising [Fig. 9(a)]. In a summary, the coating

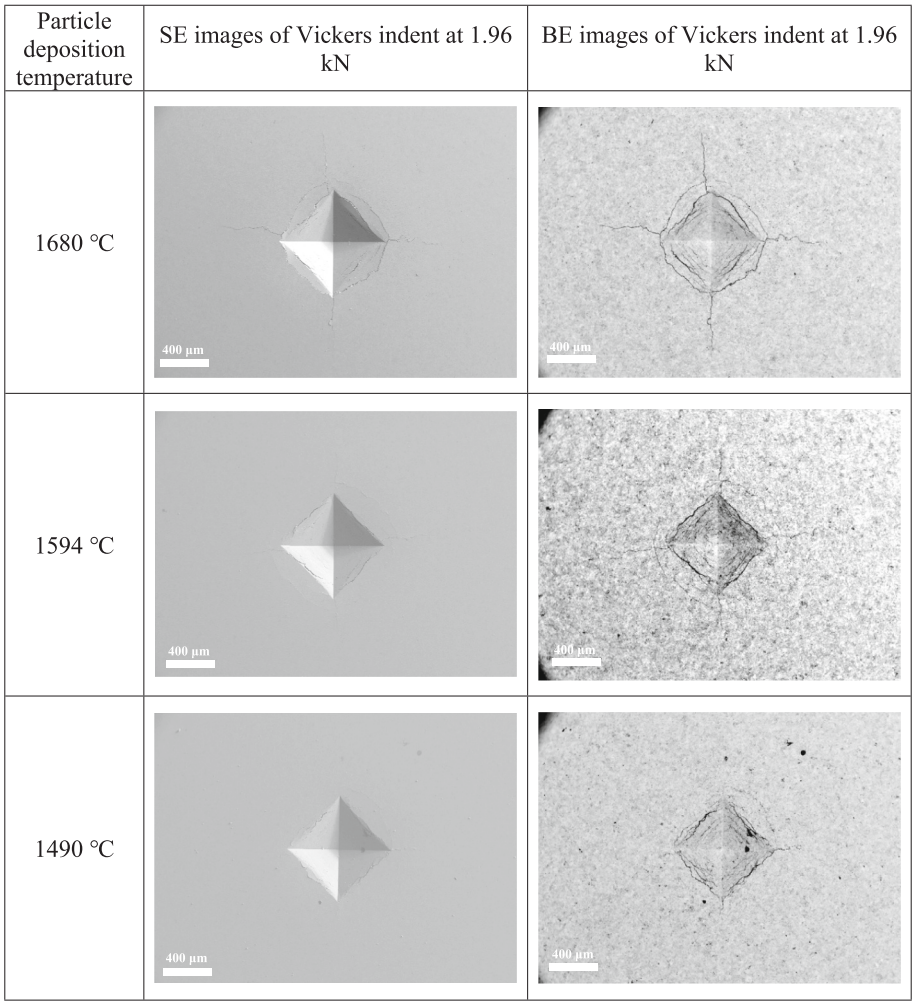

Fig. 11. The typical morphologies by both secondary electron and backscattering electron images of Vickers indents under 1.96 kN for fracture toughness measurement on the surface of WC-12Ni coatings at different particle deposition temperatures.

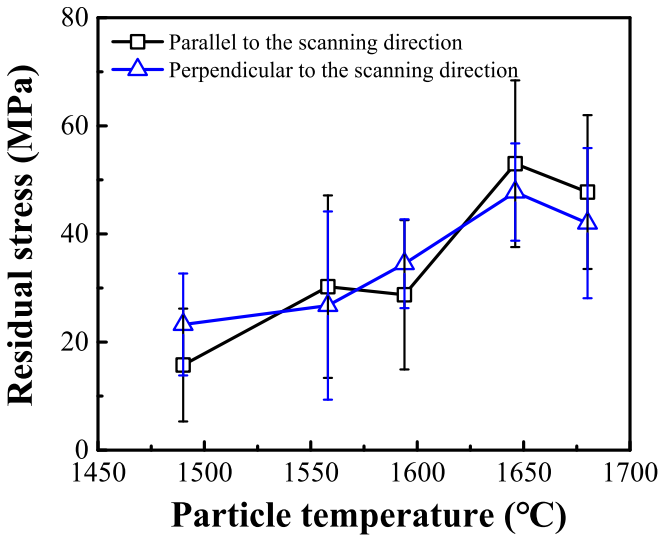

Fig. 12. Surface residual stresses of WC-12Ni coatings at the different particle deposition temperatures.

mechanical property variety of indentation fracture toughness also essentially depends on the lamellar coating microstructure, presenting a similar anisotropy in good accordance with the behaviors of hardness under small loads (Fig. 5) and elastic modulus (Fig. 8) for coating surface and cross-section.

In addition, the high-load indentation depth is larger than half of coating thickness (Table 2) by which the steel substrate was significantly involved in the indentation deformation process, i.e. being also a kind of indentation depth effect. Note that, the so-called indentation depth effect occurred only for the large load on coating surface causing excessive indent depth into the coating involving steel substrate response, distinguishing from that of indentation depth effect under small loads. Adopting the numerical analysis method in our previous study [37], the indentation process under the high load of 1.96 kN led to a maximal contact surface stress (max. Principle stress) about 6% higher for the WC-12Ni coatings with higher elastic modulus at particle deposition temperature of 1680 °C than that of the coatings at 1490 °C particle temperature. To some extent, this indentation depth effect may also promote longer cracks on the coatings of higher particle deposition temperature during the surface fracture toughness test.

4. Conclusions

In this study, a more reliable characterization of coating mechanical properties by indentation approach is considered to study the correlation of thermal spray process parameters to the properties of deposited

WC-based cemented carbide coatings, through the particle deposition temperature at almost the same particle deposition velocity. Consequently, particle temperature-dependent behaviors of coating mechanical properties along with intrinsic lamellar microstructure were probed by employing the indentation tests with Vickers and/or Berkovich instruments at a wide load range of 10^{-1}-10^{3} N order, referred as to nano-, micro- and macro-indentations, respectively, and in combination with comparative analysis of non-destructive test. The main conclusions are follows.

(1) The particle deposition temperature has a great influence on the microstructures of WC-12Ni coatings. The coating porosity decreases from 1.2% to 0.5–0.2% but WC phase decomposition is enhanced from 14% to 20% together with better splats flattening feature, as the particle deposition temperature rising from 1490 to 1680 °C. Correspondingly, a porosity divergence between coating surface and cross-section is observed with a lower coating surface porosity of 1.2–0.2% to that of cross-section of 1.2–0.5%, as a quantitative anisotropy parameter describing the intrinsic lamellar microstructure of thermal spray coatings formed by the splats flattening and piling up.

(2) Considering the coating lamellar microstructure, the indentation tests have been carried out comparatively on the coating surfaces and the cross-sections to evaluate the coating hardness and elastic modulus with small indentation loads below 3 N. For all the coatings at different particle deposition temperatures, the coating surface hardness of 12.6–13.8 GPa by nano-indentation at 650 mN, and 10.3–11.4 GPa at 0.49 N and 9.2–10.3 GPa at 2.94 N by micro-indentation, is always higher than that of the cross-section of 10.8–13.4 GPa at 650 mN, and 9.6–10.7 GPa at 0.49 N and 8.6–10.3 GPa at 2.94 N, respectively. Both the surface and cross-section hardness values increased correlatively to the particle deposition temperature rising except for the almost constant surface hardness tested below 1 N, insensitive to the particle deposition temperature. The elastic modulus by nano-indentation below 1 N also has the similar particle temperature-dependent behavior, i.e. the values on coating cross-section correlated positively to particle deposition temperature but insensitive for those on coating surface.

(3) The elastic modulus from micro-indentation with a relatively large load at 30 N on the coating surface shows the same particle deposition temperature dependence to that from nano-indentation at 650 mN on the coating cross-section, increased from 306 GPa to 364 GPa for the surface micro-indentation and from 249 GPa to 327 GPa for the cross-section nano-indenation, to the particle deposition temperature rising, respectively. Both the indentation results are in good agreement with a macro non-destructive ultrasonic test by which the coating elastic modulus is correspondingly increased from 315 GPa to 374 GPa. Moreover, the indentation fracture toughness under higher loads of 49 N on coating cross-section and 1.96 kN on coating surface is also compared and the latter presents an indentation depth effect involving steel substrate response distinguishing from that of indentation depth effect under small loads.

(4) The indentation-extracted coating mechanical properties were interpreted by that, the particle deposition temperature rising leads to the intra-splats and inter-splats defects reduction of the cemented carbides thermal spray coatings with enhanced carbide-metal bonding improvement essentially dependent on melting state of the metal binder phase. The anisotropy of the coatings with lamellar feature could be reduced either at higher temperatures or lower temperatures closely related to the melting point of the binder phase, and the coating mechanical properties are much better at the higher temperatures. Based on the clarified mechanism of particle deposition temperature, the various indentation methods may be better utilized for thermal spray coatings to probe their mechanical properties either in a localized region or over the entire coating.

CRediT authorship contribution statement

J.R. Yuan: Writing – original draft, Methodology, Formal analysis, Data curation. **X.P. Zhu:** Writing – review & editing, Supervision, Methodology, Conceptualization. **M.K. Lei:** Validation, Resources, Conceptualization.

Declaration of competing interest

The authors declare that they have no known competing financial interests or personal relationships that could have appeared to influence the work reported in this paper.

Formatting of funding sources

This work is supported by National Natural Science Foundation of China (Nos. 52371054, U21B2078) and National Key Research and Development Program of China (No. 2023YFB3408101).

Data availability

Data will be made available on request.

Acknowledgments

This work is supported by National Natural Science Foundation of China (Nos. 52371054, U21B2078) and National Key Research and Development Program of China (No. 2023YFB3408101).

References

[1] L.M. Berger, Application of hardmetals as thermal spray coatings, Int. J. Refract. Met. Hard Mater. 49 (2015) 350–364, https://doi.org/10.1016/j.ijrmhm.2014.09.029.

[2] J. García, V.C. Ciprés, A. Blomqvist, B. Kaplan, Cemented carbide microstructures: a review, Int. J. Refract. Met. Hard Mater. 80 (2019) 40–68, https://doi.org/10.1016/j.ijrmhm.2018.12.004.

[3] Z.Y. Piao, B.S. Xu, H.D. Wang, X.X. Yu, Rolling contact fatigue behavior of thermal-sprayed coating: a review, Crit. Rev. Solid State Mater. Sci. 45 (2020) 429–456, https://doi.org/10.1080/10408436.2019.1671798.

[4] K. Torkashvand, S. Joshi, M. Gupta, Advances in thermally sprayed WC-based wear-resistant coatings: co-free binders, processing routes and tribological behavior, J. Therm. Spray Technol. 31 (2022) 342–377, https://doi.org/10.1007/s11666-022-01358-4.

[5] A.R. Govande, A. Chandak, B.R. Sunil, R. Dumpala, Carbide-based thermal spray coatings: a review on performance characteristics and post-treatment, Int. J. Refract. Met. Hard Mater. 103 (2022) 105772, https://doi.org/10.1016/j.ijrmhm.2021.105772.

[6] A. Kusiak, Smart manufacturing, Int. J. Prod. Res. 56 (2018) 508–517, https://doi.org/10.1080/00207543.2017.1351644.

[7] S. Mittal, M.A. Khan, D. Romero, T. Wuest, Smart manufacturing: characteristics, technologies and enabling factors, Proc. IMechE Part B: J. Eng. Manuf. 233 (2019) 1342–1361, https://doi.org/10.1177/0954405417736547.

[8] A. Ozturk, B.M. Cetegen, Morphology of ceramic particulates formed in a premixed oxygen/acetylene flame from liquid precursor droplets, Acta Mater. 53 (2005) 2531–2544, https://doi.org/10.1016/j.actamat.2004.10.056.

[9] L. Lin, G.L. Li, H.D. Wang, J.J. Kang, Z.L. Xu, H.J. Wang, Structure and wear behavior of NiCr-Cr_3C_2 coatings sprayed by supersonic plasma spraying and high velocity oxy-fuel technologies, Appl. Surf. Sci. 356 (2015) 383–390, https://doi.org/10.1016/j.apsusc.2015.08.019.

[10] P. Suresh Babu, B. Basu, G. Sundararajan, Processing-structure-property correlation and decarburization phenomenon in detonation sprayed WC-12Co coatings, Acta Mater. 56 (2008) 5012–5026, https://doi.org/10.1016/j.actamat.2008.06.023.

[11] A.G. Bulnes, V.A. Fuentes, I.G. Cano, S. Dosta, Understanding the influence of high velocity thermal spray techniques on the properties of different anti-Wear WC-based coatings, Coatings 10 (2020) 1157, https://doi.org/10.3390/coatings10121157.

[12] A.G. Fefekos, M. Gupta, S. Mahade, S. Björklund, S. Joshi, Effect of spray angle and substrate material on formation mechanisms and properties of HVAF sprayed coatings, Surf. Coat. Technol. 452 (2023) 129115, https://doi.org/10.1016/j.surfcoat.2022.129115.

[13] I. Baumann, L. Hagen, W. Tillmann, P. Hollingsworth, D. Stangier, G. Schmidtmann, M. Tolan, M. Paulus, C. Sternemann, Process characteristics, particle behavior and coating properties during HVOF spraying of conventional,

fine and nanostructured WC-12Co powders, Surf. Coat. Technol. 405 (2021) 126716, https://doi.org/10.1016/j.surfcoat.2020.126716.
[14] K. Farokhzadeh, R.M. Fillion, A. Edrisy, The effect of deposition rate on microstructural evolution in WC-co-Cr coatings deposited by high-velocity oxy-fuel thermal spray process, J. Mater. Eng. Perform. 28 (2019) 7419–7430, https://doi.org/10.1007/s11665-019-04502-4.
[15] H.B. Wang, Q.F. Qiu, M. Gee, C. Hou, X.M. Liu, X.Y. Song, Wear resistance enhancement of HVOF-sprayed WC-co coating by complete densification of starting powder, Mater. Des. 191 (2020) 108586, https://doi.org/10.1016/j.matdes.2020.108586.
[16] K.Y. Fan, W.H. Jiang, V. Luzin, T.M. Gong, W. Feng, J. Ruiz-Hervias, P.P. Yao, Influence of WC particle size on the mechanical properties and residual stress of HVOF thermally sprayed WC-10Co-4Cr coatings, Materials 15 (2022) 5537, https://doi.org/10.3390/ma15165537.
[17] B.S. Schorr, K.J. Stein, A.R. Marder, Characterization of thermal spray coatings, Mater Charact 42 (1999) 93–100, https://doi.org/10.1016/S1044-5803(98)00048-5.
[18] S.D. Eppinger, C.D. Huber, V.H. Pham, A methodology for manufacturing process signature analysis, J. Manuf. Syst. 14 (1995) 20–34, https://doi.org/10.1016/0278-6125(95)98898-G.
[19] M.P. Sealy, Z.Y. Liu, Y.B. Guo, Z.Q. Liu, Energy based process signature for surface integrity in hard milling, J. Mater. Process. Technol. 238 (2016) 284–289, https://doi.org/10.1016/j.jmatprotec.2016.07.038.
[20] E. Brinksmeier, D. Meyer, C. Heinzel, T. Lübben, J. Sölter, L. Langenhorst, F. Frerichs, J. Kämmler, E. Kohls, S. Kuschel, Process signature-the missing link to predict surface integrity in machining, Procedia CIRP. 71 (2018) 3–10, https://doi.org/10.1016/j.procir.2018.05.006.
[21] K. Sanami, K. Shinoda, A. Yumoto, J. Akedo, Statistical evaluation of mechanical properties of thermally sprayed alumina coatings by nanoindentation method, Mater. Trans. 62 (2021) 252–260, https://doi.org/10.2320/matertrans.T-M2020866.
[22] G.M. Smith, E.J. Gildersleeve, X.T. Luo, L. Vladimir, S. Sampath, On the surface and system performance of thermally sprayed carbide coatings produced under controlled residual stresses, Surf. Coat. Technol. 387 (2020) 125536, https://doi.org/10.1016/j.surfcoat.2020.125536.
[23] V. Matikainen, H. Koivuluoto, P. Vuoristo, A study of Cr_3C_2-based HVOF-and HVAF-sprayed coatings: abrasion, dry particle erosion and cavitation erosion resistance, Wear 446 (2020) 203188, https://doi.org/10.1016/j.wear.2020.203188.
[24] S.P. Liu, Y.Q. Wang, M.X. Shen, Q. Hu, J. Xia, Y.L. Zhang, H.P. Zhao, Impact wear behavior of HVOF-sprayed WC-10Co-4Cr coating on medium carbon steel under controlled kinetic energy, J. Therm. Spray Technol. 32 (2023) 1047–1065, https://doi.org/10.1007/s11666-023-01537-x.
[25] S. Hong, J.Y. Qin, J.R. Lin, Y.P. Wu, J.H. Li, Y. Zheng, Influences of sand concentration and flow velocity on hydro-abrasive erosion behaviors of HVOF sprayed Cr_3C_2-NiCr and WC-Cr_3C_2-Ni coatings, J. Mater. Res. Technol. 21 (2022) 1507–1518.
[26] S. Houdková, O. Bláhová, F. Zahálka, M. Kašparová, The instrumented indentation study of HVOF-sprayed hardmetal coatings, J. Therm. Spray Technol. 21 (2011) 77–85, https://doi.org/10.1007/s11666-011-9677-2.
[27] J.G. La Barbera-Sosa, Y.Y. Santana, J. Caro, D. Chicot, J. Lesage, M.H. Staia, E. S. Puchi-Cabrera, Mechanical properties of WC coatings evaluated using instrumented indentation technique, Surf. Eng. 30 (2014) 498–510, https://doi.org/10.1179/1743294414Y.0000000261.
[28] X.P. Zhu, P.C. Du, Y. Meng, M.K. Lei, D.M. Guo, Solution to inverse problem of manufacturing by surface modification with controllable surface integrity correlated to performance: a case study of thermally sprayed coatings for wear performance, J. Therm. Spray Technol. 139 (2017) 061604, https://doi.org/10.1115/1.4036184.
[29] X.P. Zhu, Y. Meng, S.W. Jiang, P.C. Du, M.K. Lei, Thermal spray of cemented carbide coatings in off-angle spraying: correlations between process, coating features characteristics and performance, J. Therm. Spray Technol. 27 (2018) 1123–1142, https://doi.org/10.1007/s11666-018-0761-8.
[30] G.R. Anstis, P. Chantikul, B.R. Lawn, D.B. Marshall, A critical evaluation of indentation techniques for measuring fracture toughness: I, direct crack measurements, J. Am. Ceram. Soc. 64 (1981) 533–538, https://doi.org/10.1111/j.1151-2916.1981.tb10320.x.
[31] K. Niihara, A fracture-mechanics analysis of indentation-induced Palmqvist crack in ceramics, J. Mater. Sci. Lett. 2 (1983) 221–223, https://doi.org/10.1007/BF00725625.
[32] T. Keisuke, X-ray measurement of triaxial residual stress on machined surfaces by the cosα method using a two-dimensional detector, J. Appl. Cryst. 51 (2018) 1329–1338, https://doi.org/10.1107/S1600576718011056.
[33] J.C. Han, M. Jafari, C.G. Park, J.B. Seol, Microstructure-property relations in WC-co coatings sprayed from combinatorial Ni-plated and nanostructured powders, Mater Charact 129 (2017) 207–216, https://doi.org/10.1016/j.matchar.2017.05.005.
[34] T. Han, C.M. Deng, X.F. Zhang, Q. Liu, A model of splats deposition state and wear resistance of WC-10Co4Cr coating, Ceram. Int. 44 (2018) 4230–4236, https://doi.org/10.1016/j.ceramint.2017.12.003.
[35] S.Y. Chen, G.Z. Ma, P.F. He, Z. Liu, M. Liu, Z.G. Xing, H.D. Wang, H.J. Wang, Pore formation mechanism of WC-10Co4Cr coatings based on collected in-flight particles and individual splat, J. Inorg. Mater. 33 (2018) 895–902, https://doi.org/10.15541/jim20170518.
[36] M.K. Lei, X.P. Zhu, Y.P. Li, D.M. Guo, Significance of surface integrity on high performance manufacturing by surface modification, Int. J. Adv. Manuf. Technol. 82 (2016) 1831–1842, https://doi.org/10.1007/s00170-015-7467-6.
[37] S.J. Zhang, X.P. Zhu, J.R. Yuan, M.K. Lei, Accumulative damages of thermally sprayed cemented carbide coatings under repetitive heavy-load impacts, J. Therm. Spray Technol. 33 (2024) 275–289, https://doi.org/10.1007/s11666-024-01714-6.
[38] N.H. Faisal, R. Ahmed, A.K. Prathuru, S. Spence, M. Hossain, J.A. Steel, An improved Vickers indentation fracture toughness model to assess the quality of thermally sprayed coatings, Eng. Fract. Mech. 128 (2014) 189–204, https://doi.org/10.1016/j.engfracmech.2014.07.015.
[39] R. Ahmed, N.H. Faisal, A.M. Paradowsk, M.E. Fitzpatrick, Residual strain and fracture response of Al_2O_3 coatings deposited via APS and HVOF techniques, J. Therm. Spray Technol. 21 (2012) 23–40, https://doi.org/10.1007/s11666-011-9680-7.